ACS SENSORS

pubs.acs.org/acssensors Article

Bioelectrical Nose Platform Using Odorant-Binding Protein as a Molecular Transporter Mimicking Human Mucosa for Direct Gas Sensing

Danmin Choi, Se June Lee, Dahee Baek, So-ong Kim, Junghyun Shin, Yoonji Choi, Youngtak Cho, Sunwoo Bang, Jae Yeol Park,* Seung Hwan Lee,* Tai Hyun Park,* and Seunghun Hong*

Cite This: *ACS Sens.* 2022, 7, 3399−3408 Read Online

ACCESS | Metrics & More | Article Recommendations | Supporting Information

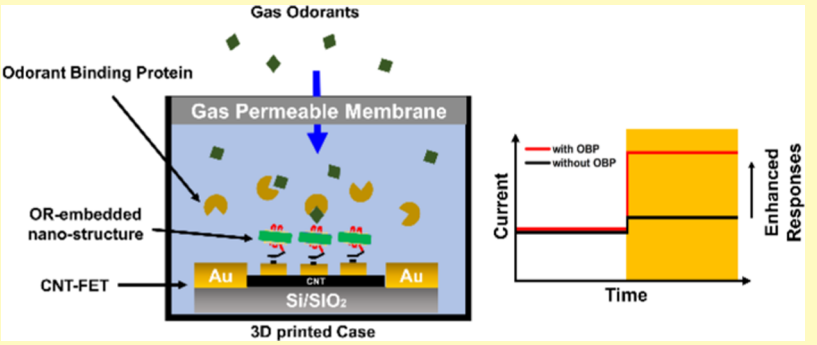

ABSTRACT: Recently, various bioelectronic nose devices based on human receptors were developed for mimicking a human olfactory system. However, such bioelectronic nose devices could operate in an aqueous solution, and it was often very difficult to detect insoluble gas odorants. Here, we report a portable bioelectronic nose platform utilizing a receptor protein-based bioelectronic nose device as a sensor and odorant-binding protein (OBP) as a transporter for insoluble gas molecules in a solution, mimicking the functionality of human mucosa. Our bioelectronic nose platform based on I7 receptor exhibited dose-dependent responses to octanal gas in real time. Furthermore, the bioelectronic platforms with OBP exhibited the sensor sensitivity improved by ∼100% compared with those without OBP. We also demonstrated the detection of odorant gas from real orange juice and found that the electrical responses of the devices with OBP were much larger than those without OBP. Since our bioelectronic nose platform allows us to directly detect gas-phase odorant molecules including a rather insoluble species, it could be a powerful tool for versatile applications and basic research based on a bioelectronic nose.

KEYWORDS: *odorant-binding protein, direct gas sensing, nanodisc, carbon nanotube field-effect transistor, biosensor platform*

An olfactory system in animal noses is used to detect certain odors such as pheromones, food flavor substances, and toxic chemicals,[1−3] which is often critical for the survival and the reproduction of various animals, plants, and insects. An important part of an olfactory system is nasal mucosa, which consists of various parts such as an epithelium, a basal membrane, and nasal mucus. A nasal mucosa humidifies and warms the air that enters a nasal cavity.[4,5] It also acts as a filter preventing the direct contact of viruses and germs with olfactory cells and protects the surface of olfactory epithelium.[6,7] The nasal mucus covers olfactory epithelial cells and includes odorant-binding proteins (OBPs) in its aqueous environment.[8] OBP molecules can bind to odorant gas molecules and help the gas molecules to be dissolved in the aqueous environment of the olfactory mucosa, which can increase the sensitivity of olfactory systems and help to detect insoluble odorant gases.[9−12]

Recently, extensive efforts have been given to build artificial nose devices, which can mimic olfactory systems. These include nanoparticle-array devices,[13,14] field-effect transistors (FETs),[15−19] nanowire devices,[20] surface plasmon resonance,[21,22] quantum dots,[23,24] and colorants.[25,26] Some of such artificial nose devices using olfactory receptor proteins as detection elements could mimic the responses of animal olfactory systems.[27,28] However, many of artificial nose devices operate only in liquid environments, requiring additional interface structures for gas detection.[29,30] Furthermore, since

Received: July 15, 2022
Accepted: October 27, 2022
Published: November 9, 2022

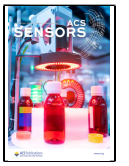

they do not have nasal mucus-like parts containing OBP, it may be very difficult to detect insoluble odorant gases.

Herein, we report a portable bioelectronic nose platform using OBP as a molecular transporter, mimicking human mucosa, for the direct sensing of odorant gases. In this study, a chamber with a gas-permeable membrane on one side was filled with an OBP solution, and a carbon nanotube FET (CNT-FET) hybridized with olfactory receptors was placed in the solution to build a bioelectronic sensor platform for direct gas detection. Here, OBP molecules were used as a vehicle transporting odorant molecules to olfactory receptor proteins on the CNT-based sensor devices. As a proof of concept, we built a bioelectronic nose device based on rat-I7 receptor, which binds to octanal as a target,[31] and demonstrated that its sensing performances were significantly improved with OBP3 molecules in the solution. The results showed that the bioelectronic noses with OBP had 10^4 times higher sensitivity and 4 times larger signals than the cases without it in the solution. In gas detection measurements, our bioelectronic noses exhibited a significantly improved sensitivity with OBP than those without it. As a proof of concept, we demonstrated the direct detection of odorant gas molecules from orange juice scent and found that the bioelectronic nose with OBP showed a higher sensitivity than those without it. Since our method allows us to evaluate insoluble gases, it could be a powerful tool for the basic research of olfaction and versatile industrial applications such as the assessment of food quality and the detection of toxic substances.

EXPERIMENTAL SECTION

Cloning of I7 and OBP3 into an Expression Vector. I7 and OBP3 genes were prepared by polymerase chain reaction (PCR) from complementary DNA clones (Origene). The genes were combined with the bacterial expression vector pET-DEST42 (invitrogen), following the manufacturer's instructions.

Expression and Purification of I7 Receptor. Rosetta 2 (DE3) cells were purchased from Novagen. The cells were transformed with the pET-DEST42 containing the I7 gene. Luria−Bertani medium (LPS solution, South Korea) was used to culture the cells with 50 μg/mL ampicillin (Sigma-Aldrich). Once the optical density value of the culture medium reached 0.5 at 600 nm, the expression of I7 was induced by injection of 1 mM isopropyl β-D-1-thiogalactopyranoside (Millipore). The cells were then further cultured and harvested (7000 rpm, 20 min). The cells were lysed by pulsed sonication (5 min), and the pellet was collected by centrifugation at 12 000 rpm for 20 min. The pellet was then suspended in a solubilization buffer. The solution was dialyzed using sodium phosphate buffer containing 0.1 M sodium phosphate and 10 mM sodium dodecyl sulfate (pH 8.0). The dialyzed solution was purified using a HisTrap HP column (Cytiva) with sodium phosphate buffer (pH 6.0 and 7.0).

Expression and Purification of OBP3. OBP3 protein was expressed using the same procedure as described for the expression of I7. After the cells were harvested, the pellet was suspended in a binding buffer containing 20 mM Tris−HCl, 20 mM imidazole, and 50 mM NaCl. The cells were lysed by pulsed sonication (5 min) and purified using a HisTrap HP column.

Expression and Purification of Membrane Scaffold Protein 1E3D1 (MSP1E3D1). Rosetta 2 (DE3) cells were transformed with the bacterial expression vector containing MSP1E3D1 (Addgene). The MSP1E3D1 protein was expressed and purified using the same procedure described for the expression of OBP3.

Construction of I7-Embedded Nanodiscs (I7-Nanodiscs). A lipid mixture (1-palmitoyl-2-oleoylphosphatidylcholine, 1-palmitoyl-2-oleoyl-*sn*-glycero-3-phosphoglycerol), I7 receptor, and MSP1E3D1 were mixed, and then bio-beads (Bio-Rad) were added to adsorb the detergent from the mixture. The mixture was incubated overnight, and I7 receptor-embedded nanodiscs were collected by size exclusion chromatography.

Intracellular Calcium Assay. HEK-293 cells were transfected with vectors containing the I7 receptor gene and cultured at 37 °C and 5% CO_2 for 48 h. The calcium indicator solution was prepared by mixing Fluo-4 AM (molecular probes) and probenecid (molecular probes) with Hanks' balanced salt solution (HBSS) buffer (Gibco). The cell culture medium of HEK-293 cells expressing I7 was replaced with HBSS buffer. Fluo-4 AM was loaded into HEK-293 cells by adding calcium indicator dye to the cells and incubating the cells at 37 °C under 5% CO_2 for 30 min. The unloaded Fluo-4 AM was washed with HBSS buffer. Subsequently, the cells were incubated for 30 min to stabilize the loaded Fluo-4 dye in the cells by changing Fluo-4 AM to Fluo-4, which is induced by intracellular esterase-mediated hydrolysis of Fluo-4 AM. The fluorescence signal was measured using a plate reader (BMG Labtech GmbH) with an excitation wavelength of 488 nm and an emission wavelength of 535 nm, and octanal was injected into the cell by the injector in the plate reader.

Ultraviolet−Visible (UV−Vis) Absorbance Measurement. Solutions were placed in a 1 × 1 × 5 cm^3 cuvette and set to a UV−vis spectroscope (Agilent 8413). The instrument's tungsten lamp and UV lamps were then turned on, and light from 180 to 1100 nm was irradiated on the cuvette. An absorbance value was calculated through the light passing through the cuvette.

Fabrication of a CNT-FET with Floating Electrodes. A CNT-FET was fabricated following the previously reported method.[32] Here, source and drain electrodes (Au (30 nm) on Ti (10 nm)) were first patterned on a Si/SiO_2 substrate via photolithography. Single-walled CNTs were dissolved in dichlorobenzene (DCB) at 0.05 mg/mL and sonicated for 3 h to prepare CNT suspensions. Then, photoresist patterns (AZ 5214E) were prepared on the substrate via photolithography, and the substrate was incubated in CNT-DCB solution overnight. Here, CNTs were adsorbed onto the bare SiO_2 regions without photoresist layers, forming CNT network-based channel on the substrate. Then, the substrate was rinsed with acetone and ethanol. Finally, floating electrodes (Au (15 nm) on Pd (10 nm)) were patterned on the CNT channel via photolithography followed by thermal evaporation. Each floating electrode had a width of 200 μm and a length of 10 μm.

Incorporation of Nanodiscs on the Floating Electrodes of CNT-FETs. Floating electrodes of CNT-FETs were functionalized with nanodisc structures following the procedure reported by our group previously.[28,33] In this process, the CNT-FET was first incubated in half V5 tag antibody solution at 37 °C for 1 h so that the antibody formed a disulfide bonding with a gold surface of the floating electrode. Then, the CNT-FET was incubated in nanodisc solution (144 μg/mL for I7-nanodiscs and 340 μg/mL for ODR-10 nanodiscs in PBS) at 37 °C for 1.5 h. Here, the nanodiscs bound to the antibody, resulting in nanodisc coatings on the floating electrodes.

Measurement of Liquid Gate Profiles of a Biofunctionalized CNT-FET. Source−drain electrodes of a CNT-FET and a liquid gate electrode were connected to a semiconductor analyzer (Keithley 4200). The 10 μL hydroxyethyl piperazine ethane sulfonic acid (HEPES) buffer was added on a CNT channel region. The source−drain bias was set to 0.1 V, and the source−drain current was measured during the gate bias voltage sweeping from −0.5 to 0.5 V.

Direct Gas Detection Using a Bioelectronic Nose. A polymer-based case of a bioelectronic nose (Figure S1) was fabricated using a 3D printer (3D Edison duo, poly(lactic acid) filament). Then, the top part of the case was covered with a gas-permeable membrane. A bioelectronic nose device was placed in the case. The interior space of the case was filled with a HEPES buffer solution with or without OBP, and the case was sealed with a rubber ring to avoid buffer leakage. For a gas sensing measurement, the fabricated case including a bioelectronic nose was placed in a closed gas chamber (acryl, 700 cm^3) with a controlled flow of various gases. The source and drain electrodes in the bioelectronic nose device were connected to a semiconductor analyzer (Keithley 4200). The source−drain bias voltage was fixed at 0.1 V, and the source-drain currents were

https://doi.org/10.1021/acssensors.2c01507
ACS Sens. 2022, 7, 3399−3408

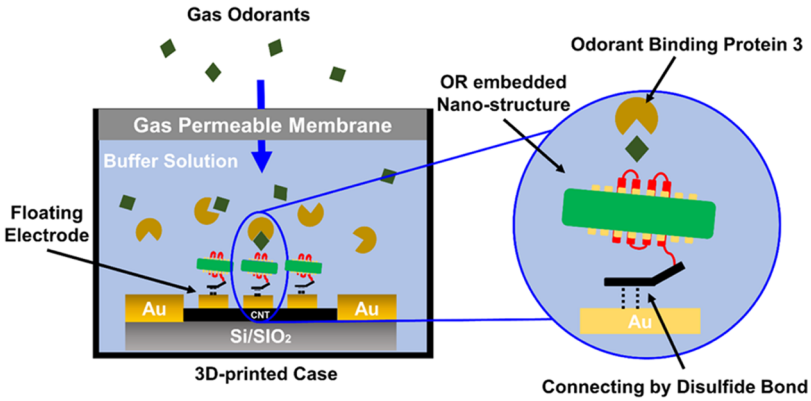

Figure 1. Schematic diagram showing a structure of a bioelectronic nose platform for the direct detection of odorant gas. Olfactory receptor-embedded nanostructures were immobilized on gold floating electrodes of the CNT-FET to build a bioelectronic nose device, and it was placed in a case filled with buffer solution. One side of the case was covered with a gas-permeable membrane to transmit the target gas while avoiding the spilling of the solution.

measured during the introduction of target gases into the gas chamber.

RESULTS AND DISCUSSION

Figure 1 shows the schematic illustration of a bioelectronic nose platform including a CNT-FET functionalized with olfactory receptor and a 3D-printed case filled with OBP solution. To build a bioelectronic nose sensor chip, a CNT-FET was functionalized with olfactory receptor-based nanostructures such as I7-nanodiscs and ODR-10 nanodiscs for the detection of specific odorant molecules as reported previously.[33−35] The detailed fabrication process of a whole platform is described in the Experimental Section. In brief, a CNT-FET that was fabricated using photolithography was functionalized with receptor containing nanostructures. The functionalized CNT-FET was fixed on the bottom part of the 3D-printed case, which is covered with a gas-permeable membrane, and the space in the 3D-printed case was filled with a buffer solution including odorant-binding protein 3 (OBP3) that is the kind of rat OBP group.[36] Odorant gas molecules passed through the gas-permeable membrane, while the membrane blocked the leakage of the buffer solution. After passing through the membrane, odorant molecules could be captured by OBP3 molecules in the buffer solution and delivered to the olfactory receptors on the CNT-FET, helping odorant molecules to bind with olfactory receptors. The binding of odorant molecules to olfactory receptors induced the conformational change of olfactory receptors as well as their charge states.[37] Eventually, it resulted in the conductance increase of a CNT channel on the CNT-FET, allowing us to monitor odorant gas molecules in real time. Our bioelectronic nose platform provides a liquid−gas interface in a portable form for the direct detection of odorant gas molecules. In addition, OBP molecules in the case were utilized to carry a rather insoluble odorant molecular species, mimicking the structure of nasal mucus in human noses.

I7 receptors and OBP3 molecules for our bioelectronic nose platforms were expressed and extracted using *Escherichia coli*, as reported previously.[9,38] Purified OBP3 and I7 were analyzed by western blotting using histidine and V5 antibodies (Figure 2a). The bands of western blot analysis for *I7* and *OBP3* revealed approximately 37 and 20 kDa, respectively; equivalent to the molecular weights of I7 and OBP3.[36,39] These results indicate that I7 and OBP3 were successfully produced using the *E. coli* system. I7 is the kind of G-protein-coupled receptor (GPCR). GPCR, as a membrane protein, has complicated structures and hydrophobicity. In this study, I7 was successively expressed using *E. coli*, which enabled the production of I7 receptors for the reconstitution of I7 receptors into nanodiscs.

Figure 2b presents the calcium fluorescence assay results showing the responses of human embryonic kidney-293 (HEK-293) cells with I7 receptor to octanal solution under different conditions. In this assay, the binding of octanal onto I7 receptor on the cells triggered the signal transduction in the cells and resulted in the increase of Ca^{2+} concentration in the cells.[31,40] Such an increase of Ca^{2+} concentration was monitored by measuring changes in the fluorescence intensity of the calcium indicator dye, Fluo-4 AM, which had been loaded in the cells. As time progressed, Ca^{2+} ions in the cytosol of the cells were pumped out by ion pumps, and the fluorescence signal of Fluo-4 decreased to the baseline level. We observed the large increase of fluorescence intensity with the introduction of octanal solution, while the OBP3 solution without octanal did not affect it much. This clearly shows that we successfully expressed the functioning I7 receptor on the cell. As a control experiment, we also performed the same assay using the cells without I7 receptor and found only negligible responses. Importantly, the cells exhibited a much larger fluorescence signal by the introduction of octanal solution with OBP3 than those without it. Presumably, the OBP3 helped the binding between octanal molecules and I7 receptors, resulting in enhanced responses.[38] Moreover, the presence of OBP3 did not affect the fluorescence signal pathway.

To confirm the binding capability of OBP3 to octanal gas, we performed the UV−vis spectroscopy (Figure 2c). Here, octanal gas (>280 ppm,[41] 2 h) was applied to deionized water and OBP3 solution in deionized water so that octanal molecules dissolved in the solution. The octanal gas was prepared by bubbling octanal solution with nitrogen gas. Since octanal has aldehyde groups, Fehling's solution could be utilized to detect octanal molecules dissolved in the solutions.[42] When Fehling's solution reacts with aldehydes in the octanal molecules, blue copper ions precipitate and turn red, which was measured using UV−vis spectroscopy. The solutions exposed to octanal gas (greed and blue lines) exhibited a much lower absorbance than those without the octanal gas exposure (red and black lines) as expected.

https://doi.org/10.1021/acssensors.2c01507
ACS Sens. 2022, 7, 3399−3408

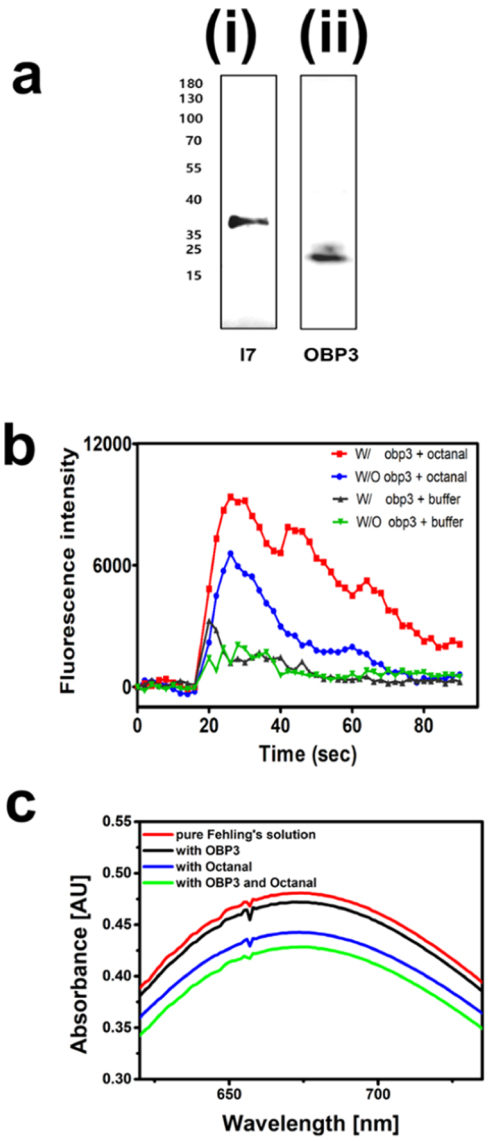

Figure 2. Characterization of I7-nanodiscs and OBP3 expressed in HEK-293 cells and *E. coli*. (a) Western blot analysis of I7 and OBP3. (b) Calcium fluorescence assay of I7-nanodiscs in response to octanal. (c) UV−vis absorbance of Fehling solutions with or without OBP3 or dissolved octanal gas.

Importantly, the absorbance of OBP3 solutions exposed to octanal was lower than that of deionized water after octanal exposure. This result clearly shows that more octanal gas molecules was dissolved in the solutions with OBP3 than those without OBP3, supporting that OBP3 can enhance the solubility of odorant gas molecules in an aqueous environment.[43]

Figure 3a illustrates the sensing experiment of octanal in solution with OBP3 using an I7-nanodisc-based bioelectronic nose device. Here, a hydroxyethyl piperazine ethane sulfonic acid (HEPES) buffer solution with or without OBP3 was first placed on the CNT channel. And, target octanal solutions with different concentrations were added to the solution while monitoring the electrical current changes of the device. The binding of octanal molecules to the I7 receptors caused a conformational change in the I7 receptor, which induced the conductance change of the CNT channel and enabled the monitoring of octanal binding events in real time.[44] This sensing experiment with or without OBP3 allowed us to evaluate the effect of OBP3 on the binding activities of octanal to the I7 receptors under aqueous environments.

The surface of a CNT-FET functionalized with I7-nanodiscs was evaluated via scanning electron microscopy (SEM). Figure 3b shows the SEM images of gold floating electrodes on a functionalized CNT-FET (i) and those with I7-nanodiscs (ii). For SEM imaging, I7-nanodiscs on gold floating electrodes were first fixed by applying OsO_4 solution to maintain their structure. Then, a thin layer of platinum (5 nm) was deposited on the device. The SEM image (ii) shows multiple spots with a circular shape and their diameters of 50−100 nm, which correspond to the dimensions of nanodiscs.[28] It indicates that I7 receptors were well-reconstituted to I7-nanodiscs without much deformation, and they were immobilized on the gold floating electrodes of the CNT-FET.

The gate profiles of a CNT-FET before and after the immobilization of I7-nanodiscs are presented in Figure 3c. Here, a voltage bias between the source and drain electrodes was set to 0.1 V, and source−drain currents were monitored during a gate voltage sweep from −0.5 to 0.5 V. When the gate voltage became more positive, the source−drain current decreased, which was a typical p-type semiconducting behavior. After the immobilization of I7-nanodiscs, the CNT-FET exhibited a decreased channel conductance with the same p-type characteristics presumably because the C-terminates of I7 receptor have positively charged amino acids.[33,45] This result indicates that the CNT-FET with I7-nanodiscs was functionalized properly and could be utilized for sensing experiments.

Figure 3d displays the real-time responses of an I7-nanodisc-based bioelectronic nose to octanal solutions with or without 1 μM OBP3. Here, the source−drain currents were measured with the source−drain bias voltage of 0.1 V during the introduction of octanal solutions from 100 pM to 10 nM in a HEPES buffer solution. A signal intensity was obtained by calculating a relative conductance change to an initial conductance ($\Delta G/G_0$). The introduction of the octanal solutions increased the channel conductance of the CNT-FET with I7-nanodiscs, as reported previously.[46] Note that the conductance changes of the CNT-FET with OBP3 were larger than those without it. These results indicate that OBP3 molecules could contribute to the binding events between octanal and I7 receptors and enhance the sensor signals. Presumably, OBP3 transported octanal molecules to I7 receptors on the CNT-FET, increasing the binding activities between I7 receptor and octanal as reported previously.[34,47] Such an increased binding activity induced the conformational rearrangement of more I7 receptors, resulting in enhanced conductance changes of the underlying CNT-FET. Note that the 1 μM OBP3 concentration used in this experiment was just 1% of that in a human olfactory system.[43] Our results show that OBP solutions with such a low concentration could significantly enhance the sensor signals. We also tested our biosensors with different concentrations of OBP3 like 0.5 and 5 μM (Figure S2). The results show that our sensors with larger concentrations of OBP3 solution indeed exhibited a larger sensor signal, clearly showing the effect of OBP3. However, from a practical point of view, higher concentrations of OBP3 should significantly increase the production cost of our sensors. Thus, the optimal concentrations of OBP3 solutions for our bioelectronic noses should be different for their applications and target molecular species.

https://doi.org/10.1021/acssensors.2c01507
ACS Sens. 2022, 7, 3399−3408

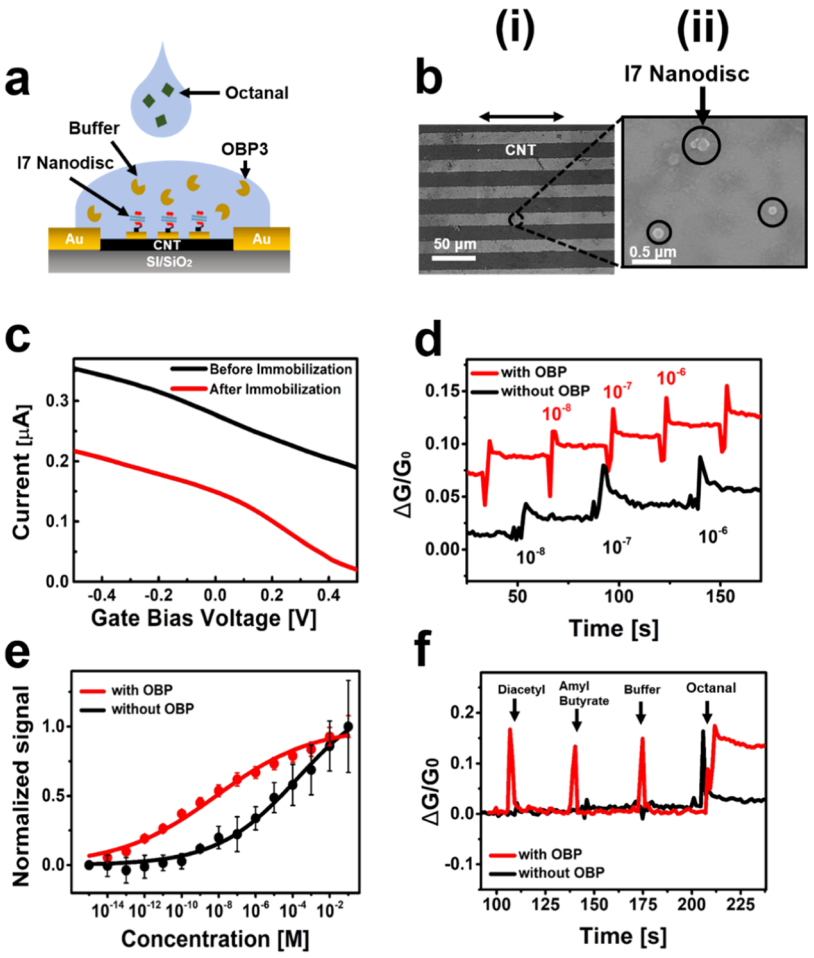

Figure 3. Sensing measurement in a buffer solution using a bioelectronic nose based on an I7-nanodisc-hybridized CNT-FET with or without OBP3. (a) Schematic illustration of sensing measurement of octanal solution with OBP3. (b) Field emission scanning electron microscopy (FESEM) images of a CNT channel (left) and I7-nanodiscs (right) immobilized on a gold floating electrode in a bioelectronic nose device. (c) Liquid gate profiles of a CNT-FET before and after the immobilization of I7-nanodiscs. The p-type profile of the CNT-FET was preserved even with nanodiscs immobilized on gold floating electrodes. (d) Real-time responses of bioelectronic nose devices with or without OBP3, to various concentrations of the octanal solution. (e) Dose-dependent responses of bioelectronic nose devices with or without OBP3 to octanal solution. Data points and error bars are averages and standard deviations of the sensor responses to each octanal concentration, respectively (n = 3). (f) Real-time responses of a bioelectronic nose device to 1 μM diacetyl, amyl butyrate, buffer, and octanal solution. In all experiments, the conductance change rate was larger with OBP3.

For more quantitative analysis, we measured the responses of I7-nanodisc-based bioelectronic noses to octanal solutions with different concentrations ranging from 10 fM to 10 mM. Figure 3e shows the normalized signals of I7-nanodisc-based bioelectronic noses to the different concentrations of octanal solutions with or without OBP3 in a HEPES buffer solution. The normalized signal was obtained by calculating the ratio of conductance changes to the maximum conductance change. Each data point and error bar were the average and the standard deviation of the sensor responses measured from three devices, respectively. These results indicate that our devices had a dose-dependent and reproducible response to octanal even with OBP3. The limit of detection (LOD) was 100 pM in the absence of OBP3, while 10 fM in the presence of OBP3, indicating an improved LOD for the sensors with OBP3. The normalized response signals N to octanal solution with different concentrations C can be fitted by a Hill equation like[48]

$$N = \frac{C^n}{C^n + EC_{50}^n} \quad (1)$$

where EC_{50} and n are the half-maximal effective concentration of the I7 receptor to octanal and Hill's coefficient, respectively. The estimated EC_{50} value for the bioelectronic nose platforms without OBP3 was around ~23.5 μM, which is similar to previously reported values.[31,40] Interestingly, with OBP3, EC_{50} value decreased down to 6.98 nM, supporting that OBP3 helped the binding between I7 receptors and ligands and enhanced the sensor sensitivity.[49] Note that the sensors with OBP3 exhibited much lower LOD and EC_{50} values than those without OBP3. In addition, the signal intensity of the sensor with OBP3 was higher than that without OBP3 in all concentrations of octanal solution. These results show that the sensor performances can be significantly increased using OBP3. Also, our sensor with OBP3 exhibited an improved detection limit compared with conventional bioelectronic noses, which used only I7 receptors without OBP3.[50,51] Our method allowed us to evaluate the effect of OBP3 on the

https://doi.org/10.1021/acssensors.2c01507
ACS Sens. 2022, 7, 3399−3408

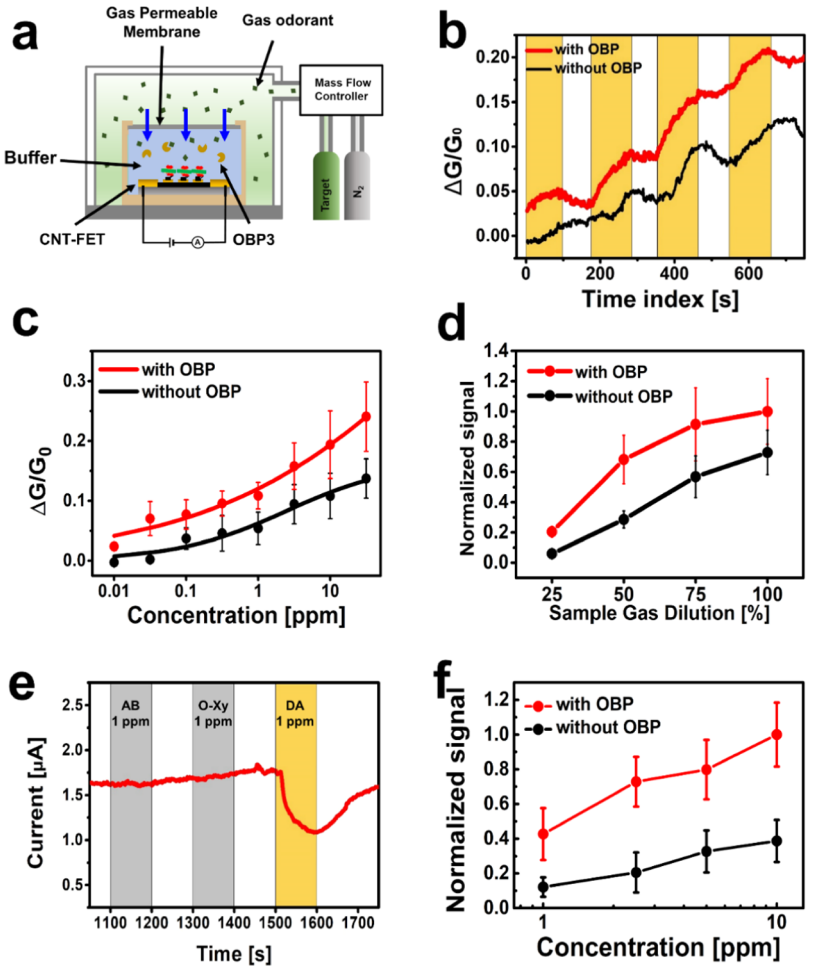

Figure 4. Direct sensing of odorant gas using a bioelectronic nose platform with or without OBP3. (a) A schematic illustration showing a setup for a direct gas sensing measurement using a bioelectronic nose platform. A sensor platform including a bioelectronic nose device in a case was placed in a gas chamber, and different mixtures of gases were introduced while monitoring the sensor signals. (b) Real-time responses of a bioelectronic nose platform with or without OBP3 to various concentrations of octanal gas. (c) Dose-dependent responses to different concentrations of the octanal gas. Data points and error bars represent averaged values and standard deviations of the data measured from three devices, respectively. (d) Normalized signals of the biomimetic odorant gas sensor to a real sample (orange) solved in DI water with four dilutions (25, 50, 75, and 100%). Data points and error bars represent averages and standard deviations of the data measured from three devices, respectively. (e) Real-time responses to amyl butyrate (AB), *ortho*-xylene (*o*-xy), and diacetyl (DA) gases. (f) Normalized signals of the bioelectronic nose that consists of an ODR-10 micelle as a receptor to different concentrations of diacetyl gas. Data points and error bars represent averages and standard deviations of the data measured from three devices, respectively.

binding behavior between olfactory receptors and odorant molecules in a quantitative manner.

We tested the selective responses of our bioelectronic nose platforms with or without OBP3 (Figure 3f). Here, diacetyl, amyl butyrate, HEPES buffer, and octanal solution at a concentration of 1 μM were consecutively introduced on the bioelectronic nose devices. During the introduction, the source−drain bias voltage was fixed at 0.1 V, and source−drain currents were monitored. The diacetyl and the amyl butyrate are butter-scented and aromatic odorants, respectively, and they do not bind to I7 receptor. Note that the conductance changes of the device were negligible at the introduction of diacetyl, amyl butyrate, and HEPES buffer solutions, while the octanal solution increased the conductance significantly. Importantly, even with OBP3, we could observe a similar selective response of our sensor devices even with an enhanced signal. These results clearly show that our platforms did not respond to nontarget molecules such as buffer or other ions, and OBP3 did not affect the selectivity in the binding events of octanal to I7 receptors. Note that this selectivity originated from the specific binding between olfactory receptors and ligands. For example, previous works about OBP-based sensors without olfactory receptors showed a rather poor selectivity of the sensors.[52,53] On the other hand, the bioelectronic sensors based on olfactory or taste receptors could discriminate similar molecular species with only a single atomic variation, indicating the high selectivity of receptor proteins.[54] Utilizing the specific binding of the receptor, our biosensor could discriminate the target from various odorant gases. In addition, the recognition of olfactory receptors depends on the structure of ligands. Therefore, even if the chemicals have a similar structure to target introduced, the device could discriminate them.[55]

To show the effect of OBP3 as a molecular transporter in our bioelectronic nose platform, we demonstrated the sensing of gas molecular species (Figure 4). Figure 4a shows a setup for a gas sensing experiment using a bioelectronic nose with OBP3. Here, our sensing platform including a bioelectronic

https://doi.org/10.1021/acssensors.2c01507
ACS Sens. 2022, 7, 3399−3408

nose device, a gas-permeable membrane, and a buffer solution with or without OBP3 was placed in a closed gas chamber. For a sensing experiment, target gas mixed with N_2 was introduced in the closed gas chamber so that target gas molecules were dissolved in the buffer solution and reached our bioelectronic sensor device. The specific binding of the target molecules onto receptors induced the conductance changes of CNT channel, which was measured as a sensor signal.

The real-time responses of an I7-nanodisc-based bioelectronic nose with or without OBP3 to octanal gas are presented in Figure 4b. The electrical responses of the bioelectronic nose were measured during the introduction of octanal gas with different concentrations ranging from 0.01 to 31 ppm. And, the signal intensity was calculated by a relative conductance change to the initial conductance of the CNT channel in the sensor device. The introduction of the octanal gas (yellow part) induced the increase of conductance change. Presumably, the octanal molecules were dissolved in a buffer solution through the gas-permeable membrane and caused the electrical responses of the sensor. Furthermore, to show that our bioelectronic nose could respond selectively to target molecules, we consecutively introduced gases of octane, *ortho*-xylene, and octanal to the chamber and monitored the responses of the sensor (Figure S3). The results show that our sensor responded only to the target gas, octanal, and the sensor signals to nontarget gases were negligible. In addition, we also confirmed that our device did not respond to other nontarget gases such as amyl butyrate and diacetyl (Figures S4 and S5). The bioelectronic noses responded to octanal gas in a dose-dependent manner. Significantly, in the presence of OBP3, relative conductance changes were enhanced by up to 100%. The result indicates that OBP3 enhanced the solubility of octanal molecules as well as the binding activity between octanal molecules and I7 receptors as reported previously.[56] When only N_2 gas was introduced without octanal gas, the relative conductance of a CNT channel decreased gradually, indicating a reversible sensing process. These results show that our bioelectronic nose with OBP3 can be used to directly detect gas-phase octanal molecules with enhanced sensitivity.

For a more detailed analysis, we measured the dose-dependent responses of I7-nanodisc-based bioelectronic noses with or without OBP3 to octanal gas (Figure 4c). Each data point and error bar were an average value and a standard deviation of the sensor signals measured from three different bioelectronic nose devices, respectively. The electrical responses of bioelectronic nose devices with or without OBP3 began to increase from 0.01 to 0.1 ppm, respectively. These results indicate that the bioelectronic nose with OBP3 responded to the octanal gas with an improved sensitivity. The data could be fitted with a Hill equation. The estimated EC_{50} value from the sensing data measured with or without OBP3 was 7.01×10^{-9} or 2.48 ppm, respectively. It supports that OBP3 enhanced the responses of our bioelectronic nose platforms. Presumably, OBP3 could enhance the solubility of octanal to the buffer solution and the reaction between octanal molecules and I7 receptors, helping the sensing process just like that in human nose systems.[57] These results represent that our system containing OBP3 could increase the responses of biosensors.

Our bioelectronic nose platform has been utilized to detect odorant gas molecules from real samples like an orange. Figure 4d shows the dose-dependent responses of bioelectronic noses with or without OBP3 to diluted odorant gas from orange juice. Here, oranges were squeezed in deionized water, and N_2 gas was bubbled in the solution to prepare a gas mixture including target odorants. This gas mixture contained octanal molecules that originally existed in orange fleshes and orange peels. Normalized response is the ratio of the signal intensity at a certain concentration to the maximum signal intensity. Data points and error bars were statistically obtained from three different bioelectronic noses. Our bioelectronic noses dose-dependently responded to sample gas from orange scent, indicating that octanal molecules could be detected by our bioelectronic nose system even in a complex gas mixture such as that from real oranges. In the presence of OBP3, the sensor signal was approximately 30% higher than that in the absence of OBP3. Presumably, OBP3 enhanced the solubility of the octanal gas molecules, increasing the sensor signals. Note that since our bioelectronic noses could be used in complex gas environments, our method can be a powerful tool for versatile applications for detection in mixed chemicals such as the qualitative evaluation of a food flavor.

As a proof of concept experiment to show the versatility of our strategy, we applied our sensing platform for bioelectronic nose devices based on other olfactory receptors. Figure 4e shows the real-time responses of an ODR-10 nanodisc-based bioelectronic nose device to the gases of amyl butyrate (AB), *ortho*-xylene (*o*-xy), or diacetyl (DA). Here, diacetyl, amyl butyrate, and *ortho*-xylene are odorants that have a buttery flavor, a pear flavor, and a sweet flavor, respectively. Only diacetyl molecules selectively bind to ODR-10 receptor as a target. For the sensing measurement, a source−drain bias voltage of the bioelectronic nose was fixed at 0.1 V, and source−drain currents were measured during the consecutive introduction of amyl butyrate, *ortho*-xylene, and diacetyl gas with 1 ppm concentration. There were negligible conductance changes for the introduction of amyl butyrate and *ortho*-xylene gases. However, when the diacetyl gas was introduced, the source−drain current decreased from approximately 1.5−1.0 μA. This result indicates that our strategy can be applied for the selective detection of target gas molecules using a bioelectronic nose device with different olfactory receptors.

Figure 4f shows the dose-dependent responses of bioelectronic noses containing an ODR-10 nanodisc-hybridized CNT-FET to diacetyl gas with or without OBP3 in a buffer solution. The normalized responses were increased as the diacetyl gas concentration increased. In the presence of OBP3, responses were approximately 20−70% higher than those without OBP3. This result indicates that our bioelectronic noses with ODR-10 nanodiscs responded to diacetyl gas molecules in a dose-dependent manner even with OBP3. Furthermore, the sensor responses were enhanced in the presence of OBP3, indicating the versatility of our strategy.

CONCLUSIONS

We have developed a bioelectronic nose platform that mimics a real olfactory system with OBP as a transporter for the direct detection of insoluble octanal gas molecules. In this work, a bioelectronic nose device was placed in a case with a gas-permeable membrane on one side. And, the case was filled with a buffer solution containing OBP3 as a transporter of insoluble gas molecules to the bioelectronic nose device. Our bioelectronic nose based on I7-nanodiscs could be used to detect octanal gas down to 0.01 ppm with OBP3, indicating an improved sensitivity with OBP3. Also, the existence of OBP3 amplified the signal intensity of our bioelectronic noses to

https://doi.org/10.1021/acssensors.2c01507
ACS Sens. 2022, 7, 3399−3408

octanal gas by ~100%. Furthermore, bioelectronic noses could be used to evaluate the octanal gas from a real orange juice scent. These results clearly show that our platform can be utilized to detect various target gases including insoluble ones with high sensitivity and selectivity just like animal noses, and it can be a useful tool for versatile applications such as the evaluation of food quality from flavor gas, the detection of toxic chemicals, and the basic research of olfactory systems.[33,58−60] In addition, since the sensor chips can be mass-produced using conventional microfabrication processes in this work,[61,62] our strategy can be utilized to integrate multiple sensors in a single chip for multiplexed detection.

■ ASSOCIATED CONTENT

Supporting Information

The Supporting Information is available free of charge at https://pubs.acs.org/doi/10.1021/acssensors.2c01507.

CAD image and photographic image of a bioelectronic nose (Figure S1); real-time responses of bioelectronic noses with various concentrations of OBP3 in buffer to octanal solution, and the responses of three bioelectronic noses with two concentrations of OBP3 to octanal solutions (Figure S2); real-time electrical responses of a bioelectronic nose with I7-nanodiscs to *ortho*-xylene, octane, and octanal gases (Figure S3); real-time electrical responses of bioelectronic noses with I7-nanodiscs to amyl butyrate gas (Figure S4); and real-time electrical responses of bioelectronic noses with I7-nanodiscs to diacetyl gas (Figure S5) (PDF)

■ AUTHOR INFORMATION

Corresponding Authors

Jae Yeol Park − *Department of Electric Vehicle, Doowon University of Technology, Paju 10838, Korea*; Email: jyp@doowon.ac.kr

Seung Hwan Lee − *Department of Bionano Engineering, Center for Bionano Intelligence Education and Research, Hanyang University, Ansan 15588, Korea*; Email: vincero78@hanyang.ac.kr

Tai Hyun Park − *School of Chemical and Biological Engineering, Institute of Chemical Processes, Seoul National University, Seoul 08826, Korea*; orcid.org/0000-0003-4254-0657; Email: thpark@snu.ac.kr

Seunghun Hong − *Department of Physics and Astronomy, Institute of Applied Physics, Seoul National University, Seoul 08826, Korea*; orcid.org/0000-0002-5176-5439; Email: seunghun@snu.ac.kr

Authors

Danmin Choi − *Department of Physics and Astronomy, Institute of Applied Physics, Seoul National University, Seoul 08826, Korea*

Se June Lee − *Department of Bionano Engineering, Center for Bionano Intelligence Education and Research, Hanyang University, Ansan 15588, Korea*

Dahee Baek − *Department of Bionano Engineering, Center for Bionano Intelligence Education and Research, Hanyang University, Ansan 15588, Korea*

So-ong Kim − *School of Chemical and Biological Engineering, Institute of Chemical Processes, Seoul National University, Seoul 08826, Korea*

Junghyun Shin − *Department of Physics and Astronomy, Institute of Applied Physics, Seoul National University, Seoul 08826, Korea*

Yoonji Choi − *Department of Physics and Astronomy, Institute of Applied Physics, Seoul National University, Seoul 08826, Korea*

Youngtak Cho − *Department of Physics and Astronomy, Institute of Applied Physics, Seoul National University, Seoul 08826, Korea*

Sunwoo Bang − *Department of Physics and Astronomy, Institute of Applied Physics, Seoul National University, Seoul 08826, Korea*

Complete contact information is available at: https://pubs.acs.org/10.1021/acssensors.2c01507

Author Contributions

S.H.L., S.J.L., and D.B. expressed OBP and reconstructed I7-nanodiscs. Y.J.C., D.C., and S.B. fabricated bioelectronic devices based on I7-nanodiscs. T.H.P. and S.-o.K. expressed and purified ODR-10 nanodiscs. Y.C fabricated bioelectronic nose devices based on ODR-10 nanodiscs. J.Y.P. designed and developed the overall structure of a bioelectronic nose platform. The main idea of this paper was conceived by J.S., Y.C., and S.H. The manuscript was mainly written by D.C., S.J.L., D.B., and Y.J.C. S.H. managed and contributed to all projects. All authors have approved the final version of the manuscript.

Funding

This work was supported by the National Research Foundation of Korea (NRF) funded by the Ministry of Science and ICT (MSIT) of Korea (Nos. 2013M3A6B2078961, 2020R1A2B5B02002152, 2018R1A2B3004498, and 2021R1F1A1062909) and the Ministry of Education (No. 2018R1A6A1A03024231). S.h.L. would like to acknowledge the support from the Technology Innovation Program funded by the Ministry of Trade, Industry & Energy (MOTIE, Korea) (No. 20008414). S.H. would like to acknowledge the support from the Ministry of Trade, Industry & Energy (MOTIE, Korea) (No. 20012390), Samsung Electronics Co., Ltd. (No. 201209-07908-01), and the European Research Council (ERC) under the European Union's Horizon 2020 program (grant agreement no. 682286).

Notes

The authors declare no competing financial interest.

■ REFERENCES

(1) Ballester, J.; Dacremont, C.; Le Fur, Y.; Etiévant, P. The role of olfaction in the elaboration and use of the Chardonnay wine concept. *Food Qual. Preference* **2005**, *16*, 351−359.

(2) Brennan, P. A.; Zufall, F. Pheromonal communication in vertebrates. *Nature* **2006**, *444*, 308−315.

(3) Hadley, K.; Orlandi, R. R.; Fong, K. J. Basic anatomy and physiology of olfaction and taste. *Otolaryngol. Clin. North Am.* **2004**, *37*, 1115−1126.

(4) Beule, A. G. Physiology and pathophysiology of respiratory mucosa of the nose and the paranasal sinuses. *GMS Curr. Top. Otorhinolaryngol. Head Neck Surg.* **2010**, *9* (SUPPL.1), S15−S34.

(5) Keck, T.; Leiacker, R.; Heinrich, A.; Kühnemann, S.; Rettinger, G. Humidity and temperature profile in the nasal cavity. *Rhinology* **2000**, *38*, 167−171.

(6) Mygind, N.; Dahl, R. Anatomy, physiology and function of the nasal cavities in health and disease. *Adv. Drug Delivery Rev.* **1998**, *29*, 3−12.

(7) Zhang, N.; Van Crombruggen, K.; Gevaert, E.; Bachert, C. Barrier function of the nasal mucosa in health and type-2 biased airway diseases. *Allergy* **2016**, *71*, 295−307.
(8) Pevsner, J.; Hou, V.; Snowman, A. M.; Snyder, S. H. Odorant-binding protein. Characterization of ligand binding. *J. Biol. Chem.* **1990**, *265*, 6118−6125.
(9) Ko, H. J.; Lee, S. H.; Oh, E. H.; Park, T. H. Specificity of odorant-binding proteins: a factor influencing the sensitivity of olfactory receptor-based biosensors. *Bioprocess Biosyst. Eng.* **2010**, *33*, 55−62.
(10) Pevsner, J.; Snyder, S. H. Odorant-binding protein: odorant transport function in the vertebrate nasal epithelium. *Chem. Senses* **1990**, *15*, 217−222.
(11) Steinbrecht, R. A. Are odorant-binding proteins involved in odorant discrimination? *Chem. Senses* **1996**, *21*, 719−727.
(12) Steinbrecht, R. A. Odorant-binding proteins: expression and function. *Ann. N. Y. Acad. Sci.* **1998**, *855*, 323−332.
(13) Oh, J.; Yang, H.; Jeong, G. E.; Moon, D.; Kwon, O. S.; Phyo, S.; Lee, J.; Song, H. S.; Park, T. H.; Jang, J. Ultrasensitive, selective, and highly stable bioelectronic nose that detects the liquid and gaseous cadaverine. *Anal. Chem.* **2019**, *91*, 12181−12190.
(14) Sharma, B.; Kim, J.-S. MEMS based highly sensitive dual FET gas sensor using graphene decorated Pd-Ag alloy nanoparticles for H2 detection. *Sci. Rep.* **2018**, *8*, No. 5902.
(15) Wang, J. Carbon-nanotube based electrochemical biosensors: A review. *Electroanal.: Int. J. Devoted Fundam. Pract. Aspects Electroanal.* **2005**, *17*, 7−14.
(16) Kim, S.; Kwak, D. H.; Choi, I.; Hwang, J.; Kwon, B.; Lee, E.; Ye, J.; Lim, H.; Cho, K.; Chung, H.-J.; Lee, W. H. Enhanced gas sensing properties of graphene transistor by reduced doping with hydrophobic polymer brush as a surface modification layer. *ACS Appl. Mater. Interfaces* **2020**, *12*, 55493−55500.
(17) Li, H.; Yin, Z.; He, Q.; Li, H.; Huang, X.; Lu, G.; Fam, D. W. H.; Tok, A. I. Y.; Zhang, Q.; Zhang, H. Fabrication of single-and multilayer MoS2 film-based field-effect transistors for sensing NO at room temperature. *Small* **2012**, *8*, 63−67.
(18) Wang, Y.; Mirkin, C. A.; Park, S.-J. Nanofabrication beyond electronics. *ACS Nano* **2009**, *3*, 1049−1056.
(19) Kim, K. H.; Moon, D.; An, J. E.; Park, S. J.; Seo, S. E.; Ha, S.; Kim, J.; Kim, K.; Phyo, S.; Lee, J.; et al. Wireless portable bioelectronic nose device for multiplex monitoring toward food freshness/spoilage. *Biosens. Bioelectron.* **2022**, *215*, No. 114551.
(20) Tang, N.; Zhou, C.; Xu, L.; Jiang, Y.; Qu, H.; Duan, X. A fully integrated wireless flexible ammonia sensor fabricated by soft nanolithography. *ACS Sens.* **2019**, *4*, 726−732.
(21) Gaggiotti, S.; Hurot, C.; Weerakkody, J. S.; Mathey, R.; Buhot, A.; Mascini, M.; Hou, Y.; Compagnone, D. Development of an optoelectronic nose based on surface plasmon resonance imaging with peptide and hairpin DNA for sensing volatile organic compounds. *Sens. Actuators, B* **2020**, *303*, No. 127188.
(22) El Kazzy, M.; Weerakkody, J. S.; Hurot, C.; Mathey, R.; Buhot, A.; Scaramozzino, N.; Hou, Y. An overview of artificial olfaction systems with a focus on surface plasmon resonance for the analysis of volatile organic compounds. *Biosensors* **2021**, *11*, No. 244.
(23) Upadhyaya, S.; Gogoi, B.; Sarma, N. S. Poly (n-vinylpyrrolidone-co-acrylonitrile-co-methacrylic acid)−graphene quantum dot conjugate: synthesis and characterization for sensing ammonia vapour. *J. Mater. Chem. C* **2021**, *9*, 2165−2177.
(24) Mirzaei, A.; Kordrostami, Z.; Shahbaz, M.; Kim, J.-Y.; Kim, H. W.; Kim, S. S. Resistive-Based Gas Sensors Using Quantum Dots: A Review. *Sensors* **2022**, *22*, No. 4369.
(25) Wang, J.; Jiang, J.; Zyryanov, G. V.; Liu, Y. A Gold Nanoparticle-Based Molecular Self-Assembled Colorimetric Chemosensor Array for Monitoring Multiple Organic Oxyanions. *Processes* **2022**, *10*, No. 1251.
(26) Bordbar, M. M.; Tashkhourian, J.; Tavassoli, A.; Bahramali, E.; Hemmateenejad, B. Ultrafast detection of infectious bacteria using optoelectronic nose based on metallic nanoparticles. *Sens. Actuators, B* **2020**, *319*, No. 128262.
(27) Goldsmith, B. R.; Mitala, J. J., Jr; Josue, J.; Castro, A.; Lerner, M. B.; Bayburt, T. H.; Khamis, S. M.; Jones, R. A.; Brand, J. G.; Sligar, S. G.; et al. Biomimetic chemical sensors using nanoelectronic readout of olfactory receptor proteins. *ACS Nano* **2011**, *5*, 5408−5416.
(28) Yang, H.; Kim, D.; Kim, J.; Moon, D.; Song, H. S.; Lee, M.; Hong, S.; Park, T. H. Nanodisc-based bioelectronic nose using olfactory receptor produced in *Escherichia coli* for the assessment of the death-associated odor cadaverine. *ACS Nano* **2017**, *11*, 11847−11855.
(29) Murugathas, T.; Zheng, H. Y.; Colbert, D.; Kralicek, A. V.; Carraher, C.; Plank, N. O. V. Biosensing with insect odorant receptor nanodiscs and carbon nanotube field-effect transistors. *ACS Appl. Mater. Interfaces* **2019**, *11*, 9530−9538.
(30) Liu, Q.; Cai, H.; Xu, Y.; Li, Y.; Li, R.; Wang, P. Olfactory cell-based biosensor: a first step towards a neurochip of bioelectronic nose. *Biosens. Bioelectron.* **2006**, *22*, 318−322.
(31) Kurland, M. D.; Newcomer, M. B.; Peterlin, Z.; Ryan, K.; Firestein, S.; Batista, V. S. Discrimination of saturated aldehydes by the rat I7 olfactory receptor. *Biochemistry* **2010**, *49*, 6302−6304.
(32) Jeong, J.-Y.; Cha, Y. K.; Ahn, S. R.; Shin, J.; Choi, Y.; Park, T. H.; Hong, S. Ultrasensitive Bioelectronic Tongue Based on the Venus Flytrap Domain of a Human Sweet Taste Receptor. *ACS Appl. Mater. Interfaces* **2022**, *14*, 2478−2487.
(33) Lee, M.; Yang, H.; Kim, D.; Yang, M.; Park, T. H.; Hong, S. Human-like smelling of a rose scent using an olfactory receptor nanodisc-based bioelectronic nose. *Sci. Rep.* **2018**, *8*, No. 13945.
(34) Lee, M.; Jung, J. W.; Kim, D.; Ahn, Y.-J.; Hong, S.; Kwon, H. W. Discrimination of umami tastants using floating electrode-based bioelectronic tongue mimicking insect taste systems. *ACS Nano* **2015**, *9*, 11728−11736.
(35) Kim, B.; Lee, J.; Namgung, S.; Kim, J.; Park, J. Y.; Lee, M.-S.; Hong, S. DNA sensors based on CNT-FET with floating electrodes. *Sens. Actuators, B* **2012**, *169*, 182−187.
(36) Löbel, D.; Strotmann, J.; Jacob, M.; Breer, H. Identification of a third rat odorant-binding protein (OBP3). *Chem. Senses* **2001**, *26*, 673−680.
(37) Rubenstein, L. A.; Lanzara, R. G. Activation of G protein-coupled receptors entails cysteine modulation of agonist binding. *J. Mol. Struct.: THEOCHEM* **1998**, *430*, 57−71.
(38) Ko, H. J.; Park, T. H. Enhancement of odorant detection sensitivity by the expression of odorant-binding protein. *Biosens. Bioelectron.* **2008**, *23*, 1017−1023.
(39) Minic, J.; Persuy, M. A.; Godel, E.; Aioun, J.; Connerton, I.; Salesse, R.; Pajot-Augy, E. Functional expression of olfactory receptors in yeast and development of a bioassay for odorant screening. *FEBS J.* **2005**, *272*, 524−537.
(40) Araneda, R. C.; Peterlin, Z.; Zhang, X.; Chesler, A.; Firestein, S. A pharmacological profile of the aldehyde receptor repertoire in rat olfactory epithelium. *J. Physiol.* **2004**, *555*, 743−756.
(41) Verevkin, S. P.; Krasnykh, E. L.; Vasiltsova, T. V.; Koutek, B.; Doubsky, J.; Heintz, A. Vapor pressures and enthalpies of vaporization of a series of the linear aliphatic aldehydes. *Fluid Phase Equilib.* **2003**, *206*, 331−339.
(42) Fehling, H. Die quantitative Bestimmung von Zucker und stärkmehl mittelst Kupfervitriol. *Justus Liebigs Ann. Chem.* **1849**, *72*, 106−113.
(43) Pelosi, P. Odorant-binding proteins. *Crit. Rev. Biochem. Mol. Biol.* **1994**, *29*, 199−228.
(44) Hollmann, M. W.; Strumper, D.; Herroeder, S.; Durieux, M. E.; Warltier, D. C. Receptors, G proteins, and their interactions. *J. Am. Soc. Anesthesiol.* **2005**, *103*, 1066−1078.
(45) Hall, S. E.; Floriano, W. B.; Vaidehi, N.; Goddard, W. A. Predicted 3-D structures for mouse I7 and rat I7 olfactory receptors and comparison of predicted odor recognition profiles with experiment. *Chem. Senses* **2004**, *29*, 595−616.
(46) Lee, S. H.; Lee, M.; Yang, H.; Cho, Y.; Hong, S.; Park, T. H. Bioelectronic sensor mimicking the human neuroendocrine system for the detection of hypothalamic-pituitary-adrenal axis hormones in human blood. *Biosens. Bioelectron.* **2020**, *154*, No. 112071.

https://doi.org/10.1021/acssensors.2c01507
ACS Sens. 2022, 7, 3399−3408

(47) Pes, D.; Pelosi, P. Odorant-binding proteins of the mouse. *Comp. Biochem. Physiol., Part B: Biochem. Mol. Biol.* **1995**, *112*, 471−479.
(48) Neubig, R. R.; Spedding, M.; Kenakin, T.; Christopoulos, A. International Union of Pharmacology Committee on Receptor Nomenclature and Drug Classification. XXXVIII. Update on terms and symbols in quantitative pharmacology. *Pharmacol. Rev.* **2003**, *55*, 597−606.
(49) Vidic, J.; Grosclaude, J.; Monnerie, R.; Persuy, M.-A.; Badonnel, K.; Baly, C.; Caillol, M.; Briand, L.; Salesse, R.; Pajot-Augy, E. On a chip demonstration of a functional role for odorant binding protein in the preservation of olfactory receptor activity at high odorant concentration. *Lab Chip* **2008**, *8*, 678−688.
(50) Ko, H. J.; Park, T. H. Piezoelectric olfactory biosensor: ligand specificity and dose-dependence of an olfactory receptor expressed in a heterologous cell system. *Biosens. Bioelectron.* **2005**, *20*, 1327−1332.
(51) Lee, S. H.; Ko, H. J.; Park, T. H. Real-time monitoring of odorant-induced cellular reactions using surface plasmon resonance. *Biosens. Bioelectron.* **2009**, *25*, 55−60.
(52) Larisika, M.; Kotlowski, C.; Steininger, C.; Mastrogiacomo, R.; Pelosi, P.; Schütz, S.; Peteu, S. F.; Kleber, C.; Reiner-Rozman, C.; Reiner-Rozman, C.; Nowak, C. Electronic olfactory sensor based on *A. mellifera* odorant-binding protein 14 on a reduced graphene oxide field-effect transistor. *Angew. Chem., Int. Ed.* **2015**, *54*, 13245−13248.
(53) Lu, Y.; Yao, Y.; Zhang, Q.; Zhang, D.; Zhuang, S.; Li, H.; Liu, Q. Olfactory biosensor for insect semiochemicals analysis by impedance sensing of odorant-binding proteins on interdigitated electrodes. *Biosens. Bioelectron.* **2015**, *67*, 662−669.
(54) Lee, S. H.; Jin, H. J.; Song, H. S.; Hong, S.; Park, T. H. Bioelectronic nose with high sensitivity and selectivity using chemically functionalized carbon nanotube combined with human olfactory receptor. *J. Biotechnol.* **2012**, *157*, 467−472.
(55) Kim, T. H.; Lee, S. H.; Lee, J.; Song, H. S.; Oh, E. H.; Park, T. H.; Hong, S. Single-carbon-atomic-resolution detection of odorant molecules using a human olfactory receptor-based bioelectronic nose. *Adv. Mater.* **2009**, *21*, 91−94.
(56) Tegoni, M.; Pelosi, P.; Vincent, F.; Spinelli, S.; Campanacci, V.; Grolli, S.; Ramoni, R.; Cambillau, C. Mammalian odorant binding proteins. *Biochim. Biophys. Acta, Protein Struct. Mol. Enzymol.* **2000**, *1482*, 229−240.
(57) Briand, L.; Eloit, C.; Nespoulous, C.; Bézirard, V.; Huet, J.-C.; Henry, C.; Blon, F.; Trotier, D.; Pernollet, J.-C. Evidence of an odorant-binding protein in the human olfactory mucus: location, structural characterization, and odorant-binding properties. *Biochemistry* **2002**, *41*, 7241−7252.
(58) Kovács, Z.; Dalmadi, I.; Lukács, L.; Sipos, L.; Szántai-Kőhegyi, K.; Kókai, Z.; Fekete, A. Geographical origin identification of pure Sri Lanka tea infusions with electronic nose, electronic tongue and sensory profile analysis. *J. Chemom.* **2010**, *24*, 121−130.
(59) Zhang, Y.-c.; Gao, S.-s.; Xue, S.; Zhang, K.-p.; Wang, J.-s.; Li, B. Odorant-binding proteins contribute to the defense of the red flour beetle, *Tribolium castaneum*, against essential oil of *Artemisia vulgaris*. *Front. Physiol.* **2020**, *11*, No. 819.
(60) Shin, N.; Lee, S. H.; Pham Ba, V. A.; Park, T. H.; Hong, S. Micelle-stabilized olfactory receptors for a bioelectronic nose detecting butter flavors in real fermented alcoholic beverages. *Sci. Rep.* **2020**, *10*, No. 9064.
(61) McGill, S. A.; Rao, S. G.; Manandhar, P.; Xiong, P.; Hong, S. High-performance, hysteresis-free carbon nanotube field-effect transistors via directed assembly. *Appl. Phys. Lett.* **2006**, *89*, No. 163123.
(62) Gao, Z.; Kang, H.; Naylor, C. H.; Streller, F.; Ducos, P.; Serrano, M. D.; Ping, J.; Zauberman, J.; et al. Scalable production of sensor arrays based on high-mobility hybrid graphene field effect transistors. *ACS Appl. Mater. Interfaces* **2016**, *8*, 27546−27552.

https://doi.org/10.1021/acssensors.2c01507
ACS Sens. 2022, 7, 3399−3408